21st Australasian Fluid Mechanics Conference
Adelaide, Australia
10-13 December 2018

Examination of the Details of 2D Vorticity Generation Around the Airfoil During Starting and Stopping Phases

Alwin R. Wang and Hugh M. Blackburn

Department of Mechanical and Aerospace Engineering
Monash University, Victoria 3800, Australia

Abstract

This paper presents a numerical study of vorticity generation around a 2D airfoil during the starting and stopping phases of motion. The study focuses on a single NACA0012 airfoil of unit chord at 4° angle of attack where the two-dimensional Navier-Stokes equations are solved using a spectral element DNS code. Peaks in the boundary vorticity flux on the trailing edge surface support recent findings about the establishment of the Kutta condition. The peaks in lift force during the starting and stopping phases appear to be well-explained by thin airfoil theory for non-uniform motion while the peaks in the drag force appear well-explained by vortex impulse and added mass.

Introduction

Around 1930, Prandtl, Tietjens and Müller recorded the motion of fine particles around an airfoil in the starting and stopping phases of motion to observe transient, unsteady flows [9]. The original recordings have been analysed using modern particle image velocimetry by Willert and Kompenhans [14] and the starting and stopping vortices still remain of interest.

Vincent and Blackburn [12] showed the formation of these vortices by performing a direct numerical simulation (DNS) of transient flow over a NACA0012 airfoil at $\mathrm{Re} = 10,000$ and $\alpha = 4^\circ$ while Agromayo, Rúa and Kristoffersen [1] investigated a NACA4612 at $\mathrm{Re} = 1,000$ and $\alpha = 16^\circ$ using OpenFOAM. Both studies determined coefficients of lift and drag during the starting and stopping phases and verified Kelvin's and Stoke's theorems, shown in equation (1), for vorticity around various contours. This paper expands on these studies by considering the vorticity generation mechanisms and exploring the physical phenomena behind vortices generated during the starting and stopping phases.

$$\Gamma = \oint_C \vec{V}\cdot \mathrm{d}\vec{l} = \iint_S \vec{\nabla}\times\vec{v}\cdot \mathrm{d}S = \iint_S \vec{\omega}\cdot \mathrm{d}\vec{S} \tag{1}$$

It is recognised that the sources of vorticity must occur at the boundary of the fluid regions. For the starting and starting phases of motion, Morton [10] outlines two production mechanisms for vorticity as shown in equation (2): tangential pressure gradients from the fluid side and the acceleration of the surface from the wall side. These contributions were investigated by Blackburn and Henderson [3] for vortex shedding of oscillating cylinders and it was noted that the pressure-gradient generation mechanism could override the surface-acceleration generation mechanism and vice versa.

$$-\nu\left(\frac{\partial\vec{\omega}}{\partial z}\right)_0 = -\frac{1}{\rho}\left[\left(\vec{n}\times\nabla\right)\vec{p}\right]_0 - \vec{n}\times\frac{\mathrm{d}V}{\mathrm{d}t} \tag{2}$$

Zhu et al. [16] investigated the causal mechanisms for airfoil circulation using vorticity creation theory based on Lighthill's relations [6], instead of boundary-layer theory. The realisation of the Kutta condition and creation of starting vortex were determined through a complex chain of processes explained by considering the vorticity and boundary vorticity flux, σ.

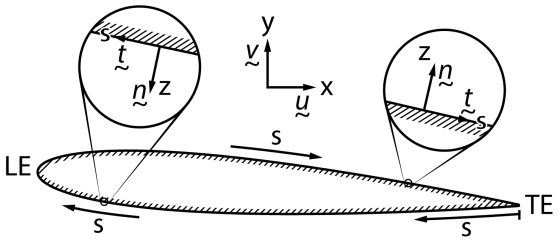

Figure 1: Coordinate system used in this analysis

Another point of interest identified by Vincent and Blackburn [12] and Agromayo, Rúa and Kristoffersen [1] was the large value of lift during the starting (accelerating) phase. Kármán and Sears [5] attributed this to unsteady flows over airfoils which was later extended by Liu et al. [8] and Limacher, Morton and Wood [7]. After the starting phase, when the airfoil had attained a uniform velocity, it was also observed the lift force would asymptote to a steady-state value. An explanation for this was also provided by Kármán and Sears [5] due to a "lift deficiency" term from the effect of wake vorticity sheet generated during acceleration. This behaviour was also detailed by Saffman explaining latency in lift production known as the "Wagner effect" [11, 13].

Both of these effects will also be investigated in this study of vorticity production as the vorticity is not contained to a thin region.

Numerical Method

Governing Equations and Numerical Approach

Simulation was carried out using the Semtex code [4] which is a spectral element-Fourier DNS code. The governing equations solved were the non-dimensionalised Navier-Stokes equations in the moving reference frame fixed to the airfoil,

$$\nabla\cdot\vec{u} = 0 \tag{3}$$

$$\frac{\partial\vec{u}}{\partial t} + \vec{u}\cdot\nabla\vec{u} = -\nabla\vec{P} + \frac{1}{\mathrm{Re}}\nabla^2\vec{u} - a \tag{4}$$

where $\vec{P} = \frac{\vec{p}}{\rho}$ and a is the acceleration of the reference frame. The velocity boundary condition was set as $u = -V(t)$ where $V(t)$ is the velocity of the reference frame such that $a = V'(t)$.

For motion of a two-dimensional plane boundary moving in its own plane with velocity $V = (V(t), 0)$, the diffusive flux density (flow per unit length per unit time) of positive vorticity outwards from the wall was given as:

$$-\sigma \equiv -\nu\frac{\partial\vec{\omega}}{\partial z}\Big|_{z=0} = -\vec{n}\times\left(\nabla\vec{P} + \vec{a}\right) \tag{5}$$

where $\vec{\omega}$ was the vorticity, $\vec{n}$ was the unit wall-normal vector, z was the distance normal to the surface and $\vec{a}$ was the local wall acceleration [10]. The term boundary vorticity flux (BVF), σ, has been introduced based on Zhu et al. [16].

It was assumed that a local section of airfoil could be modelled as an infinite plane with negligible curvature and the acceleration of the plane was given by $\vec{t}\cdot\vec{a}$ where $\vec{t}$ was a unit tangent vector as shown in figure 1. Thus, the vorticity production around the airfoil was given by equation 6 for a particular point on the airfoil.

$$-\nu\frac{\partial\omega}{\partial z} = -\frac{1}{\rho}\frac{\partial p}{\partial s} - \vec{t}\cdot\vec{a} \tag{6}$$

It was clear that the convergence of second derivatives for u and v were required to accurately determine $\nabla\vec{\omega}$. The acceleration profile for the airfoil was chosen to be the same as that of Vincent and Blackburn [12] which represents non-impulsively started flow to a unity free-stream velocity (figure 2).

Grid and Time Step Refinement

To determine an appropriate choice for the order of the tensor-product GLL shape functions used in each spectral element, tests were conducted at $t = 0.15\,\mathrm{s}$ which corresponded to the maximum forwards (negative) acceleration of the airfoil. A p-Convergence test where p is the order of the tensor-product was performed. Values of p between 3 and 18 were used and their results compared to $p = 19$ and the result is shown in figure 3. A value of $p = 10$ was chosen.

The final spectral element mesh used had 989 conforming quadrilateral spectral elements as shown in figure (4). Local mesh refinement was concentrated near the surface of the airfoil to resolve the boundary layer and at the trailing edge to resolve the BVF. 10^{th}-order tensor-product nodal basis functions were used in each element, giving a total of 98,900 independent mesh nodes.

Unsteady Thin-Airfoil Theory

According to classic thin airfoil theory provided in Anderson [2] the vortex sheet strength of an airfoil, $\gamma(\xi)$, could be determined as

$$\frac{1}{2\pi}\int_{-1}^{1}\frac{\gamma(\xi)}{x-\xi}\,\mathrm{d}\xi = V_\infty\left(\alpha - \frac{\mathrm{d}z}{\mathrm{d}x}\right) \tag{7}$$

where the terminals have been adjusted to match the definition provided in [5] and $\frac{\mathrm{d}z}{\mathrm{d}x} = 0$ in this analysis for a symmetric airfoil. This could be applied to Kármán and Sears [5] derivation for the lift of a thin airfoil in non-uniform motion:

$$L = \underbrace{\rho V_\infty \Gamma_0}_{\text{Quasi-Steady}} - \underbrace{\rho\frac{\mathrm{d}}{\mathrm{d}t}\int_{-1}^{1}\gamma_0(x)\,x\,\mathrm{d}x}_{\text{Apparent Mass}} - \underbrace{\rho V_\infty\int_{1}^{\infty}\gamma(\varepsilon)\frac{\mathrm{d}\varepsilon}{\sqrt{\varepsilon^2-1}}}_{\text{Wake Effect}} \tag{8}$$

where $\gamma_0(x)$ and Γ_0 were the vortex sheet strength and circulation respectively, calculated from thin airfoil theory. $\gamma(\varepsilon)$ was the vorticity of the wake assumed to be on the airfoil plane a distance ε from the mid-chord ($x = 0$).

While Kármán and Sears [5] presented a solution for the wake effect term, from PIV by Willert and Kompenhans [14] it was clear the assumption of the wake remaining in the same plane as the airfoil did not hold as wake vortex sheet rolls up to form the starting vortex. Thus, only the first two terms, quasi-steady state, L_0, and apparent mass, L_1, were investigated.

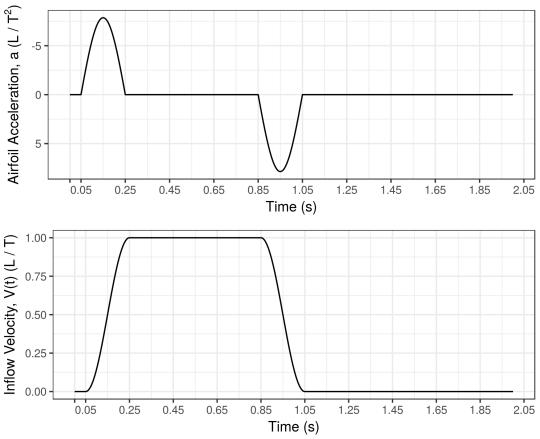

Figure 2: Airfoil during the starting and stopping phases

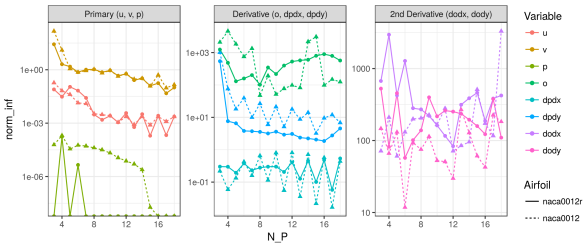

Figure 3: p-Convergence study results

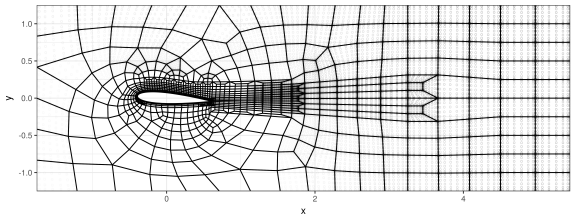

Figure 4: Spectral element mesh used

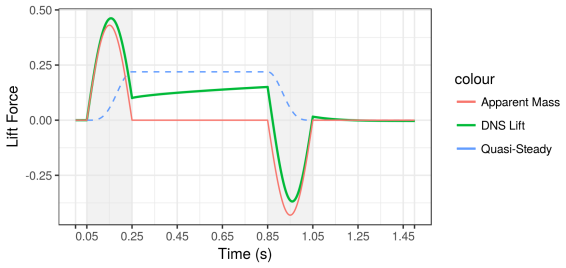

Figure 5: Unsteady lift estimation using equation (8)

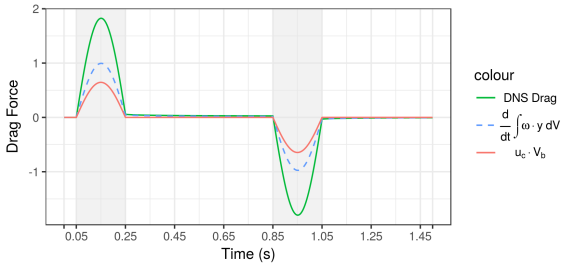

Figure 6: Added mass force for drag using equation (9)

Added Mass Force

When the no slip condition holds, Limacher, Morton and Wood [7] stated that $\vec{P}_i + \vec{P}_\Phi = 0$, which led to their second expression for vortex impulse $\vec{P}$, where $\vec{F} = -\rho \frac{\mathrm{d}\vec{P}}{\mathrm{d}t}$. This could be used to determine the lift and drag forces based on the shed-vorticity impulse, $\vec{P}_v$, and the body-volume impulse, $\vec{P}_b$, and could explain the high values observed.

$$\vec{P} = \vec{P}_v + \vec{P}_b = \int_V (\vec{x} \times \vec{\omega}) \, \mathrm{d}V - \vec{u}_c V_b \tag{9}$$

Results and Discussion

Starting Vortex and Establishing the Kutta Condition

In figure 7 it can be seen that in the second half of the starting phase, $t \in [0.15, 0.25]\,\mathrm{s}$, the vorticity on the upper and lower surfaces are not equal. When $t \in [0.25, 0.85]\,\mathrm{s}$ it can be seen that the vorticity on the upper and lower surfaces approach each other and, given sufficient time, are equal at the trailing edge satisfying the Kutta condition. In comparison, it is noted that the leading edge vorticity appears to have reached a steady-state value much faster.

When analysing the key stages in establishing the Kutta condition, Zhu et al. [16] recognised the importance of sharp BVF peaks on both sides of the trailing edge. These peaks are also present in this non-impulsively-started flow as shown in figure 8 which supports this argument.

However, the BVF in figure 8 does not alternate signs which would indicate the formation of a vortex bubble at the trailing edge. Zhu et al. [16] and Xu [15] identified the vortex bubble as a key stage in the development of non-impulsively started flows which suggests there is insufficient resolution at the trailing edge in this DNS. Both Zhu and Xu used alternate solvers.

The leading edge also has sharp BVF peaks that vary with time during the stopping phase, $t \in [0.85, 1.05]\,\mathrm{s}$, in a similar fashion to the trailing edge. This could contribute to the formation of leading edge stopping vortices observed.

Unsteady Thin-Airfoil Theory

Figure 5 compares the quasi-steady and apparent mass terms of equation (8) with the result from DNS. Immediately it is clear that apparent mass is the major contributor to the large lift force during the starting and stopping phases. At the end of the stopping phase, the DNS lift is approximately one half of the quasi-steady lift. This is in agreement with Saffman's statement that the initial lift is one-half of the final steady-state lift [11].

Added Mass Force

Applying equation (9) to the flow field at each time step yields figure 6 for the drag force. It is clear that the majority of the drag force is due to the shed-vorticity impulse, $\vec{P}_v$, with the body-volume impulse, $\vec{P}_b$, only having an effect during the starting and stopping motions. This is consistent with Limacher, Morton and Wood [7] as $\vec{P}_b$ is an added-mass force which should only be present in non-steady flow.

Conclusions

This paper further develops the study of vorticity generation mechanisms by applying them to the starting and stopping phases of airfoil motion. The results corroborate phenomena observed by other authors in a non-impulsively-started flow. Unsteady thin airfoil theory was also applied to explain the lift forces observed during the starting and stopping phases. The added mass force was used to explain the peaks in drag.

References

[1] Agromayor, R., Rúa, J. and Kristoffersen, R., Simulation of Starting and Stopping Vortices of an Airfoil, in *Proceedings of the 58th Conference on Simulation and Modelling (SIMS 58) Reykjavik, Iceland, September 25th – 27th, 2017*, Linkoping University Electronic Press, 2017.

[2] Anderson, J. D., *Fundamentals of Aerodynamics*, Aeronautical and Aerospace Engineering Series, McGraw-Hill, 2010, 5th edition.

[3] Blackburn, H. M. and Henderson, R. D., A study of two-dimensional flow past an oscillating cylinder, *Journal of Fluid Mechanics*, **385**, 1999, 255–286.

[4] Blackburn, H. M. and Sherwin, S. J., Formulation of a Galerkin spectral element–Fourier method for three-dimensional incompressible flows in cylindrical geometries, *Journal of Computational Physics*, **197**, 2004, 759–778.

[5] Kármán, T. V. and Sears, W. R., Airfoil Theory for Non-Uniform Motion, *Journal of the Aeronautical Sciences*, **5**, 1938, 379–390.

[6] Lighthill, J., *An Informal Introduction to Theoretical Fluid Mechanics*, Oxford University Press, 1986.

[7] Limacher, E., Morton, C. and Wood, D., Generalized derivation of the added-mass and circulatory forces for viscous flows, *Physical Review Fluids*, **3**.

[8] Liu, T., Wang, S., Zhang, X. and He, G., Unsteady Thin-Airfoil Theory Revisited: Application of a Simple Lift Formula, *AIAA Journal*, **53**, 2015, 1492–1502.

[9] Ludwig Prandtl, O. K. G. T., *Applied hydro- and aeromechanics*, New York; London : McGraw-Hill Book Company, inc., 1934, 1st edition, plates: p. 277-306.

[10] Morton, B. R., The generation and decay of vorticity, *Geophysical & Astrophysical Fluid Dynamics*, **28**, 1984, 277–308.

[11] Saffman, P. G., *Vortex Dynamics (Cambridge Monographs on Mechanics)*, Cambridge University Press, 1993.

[12] Vincent, M. and Blackburn, H. M., Simulation of starting/stopping vortices for a lifting aerofoil, in *Proceedings of the 19th Australasian Fluid Mechanics Conference (AFMC)*, editors H. Chowdhury and F. Alam, RMIT University, 2014.

[13] Wagner, H., Über die Entstehung des dynamischen Auftriebes von Tragflügeln, *ZAMM - Zeitschrift für Angewandte Mathematik und Mechanik*, **5**, 1925, 17–35.

[14] Willert, C. and Kompenhans, J., PIV Analysis of Ludwig Prandtl's Historic Flow Visualization Films, *arXiv preprint*.

[15] Xu, L., Numerical study of viscous starting flow past wedges, *Journal of Fluid Mechanics*, **801**, 2016, 150–165.

[16] Zhu, J. Y., Liu, T. S., Liu, L. Q., Zou, S. F. and Wu, J. Z., Causal mechanisms in airfoil-circulation formation, *Physics of Fluids*, **27**, 2015, 123601.

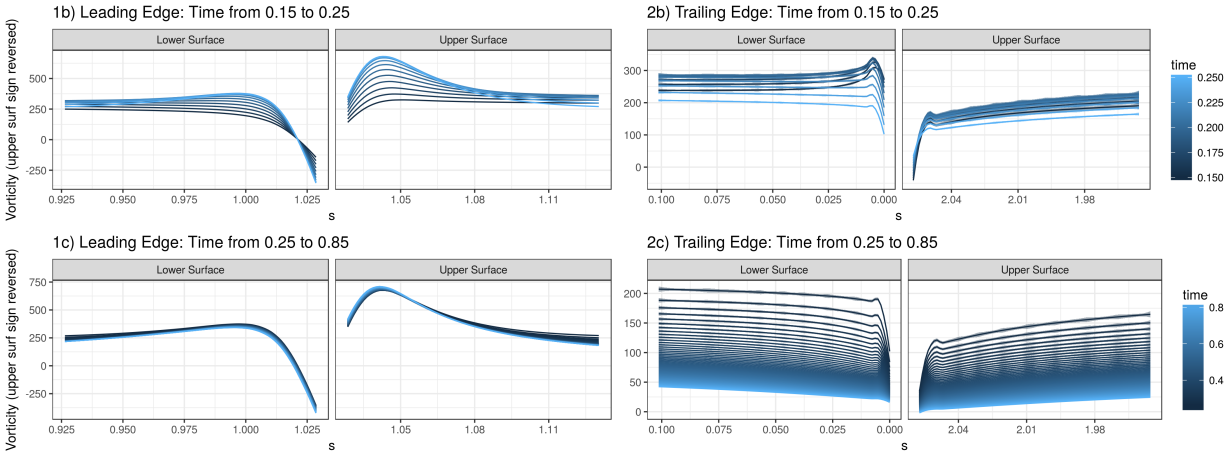

Figure 7: Vorticity on the airfoil surface for the first and last 10% of the chord

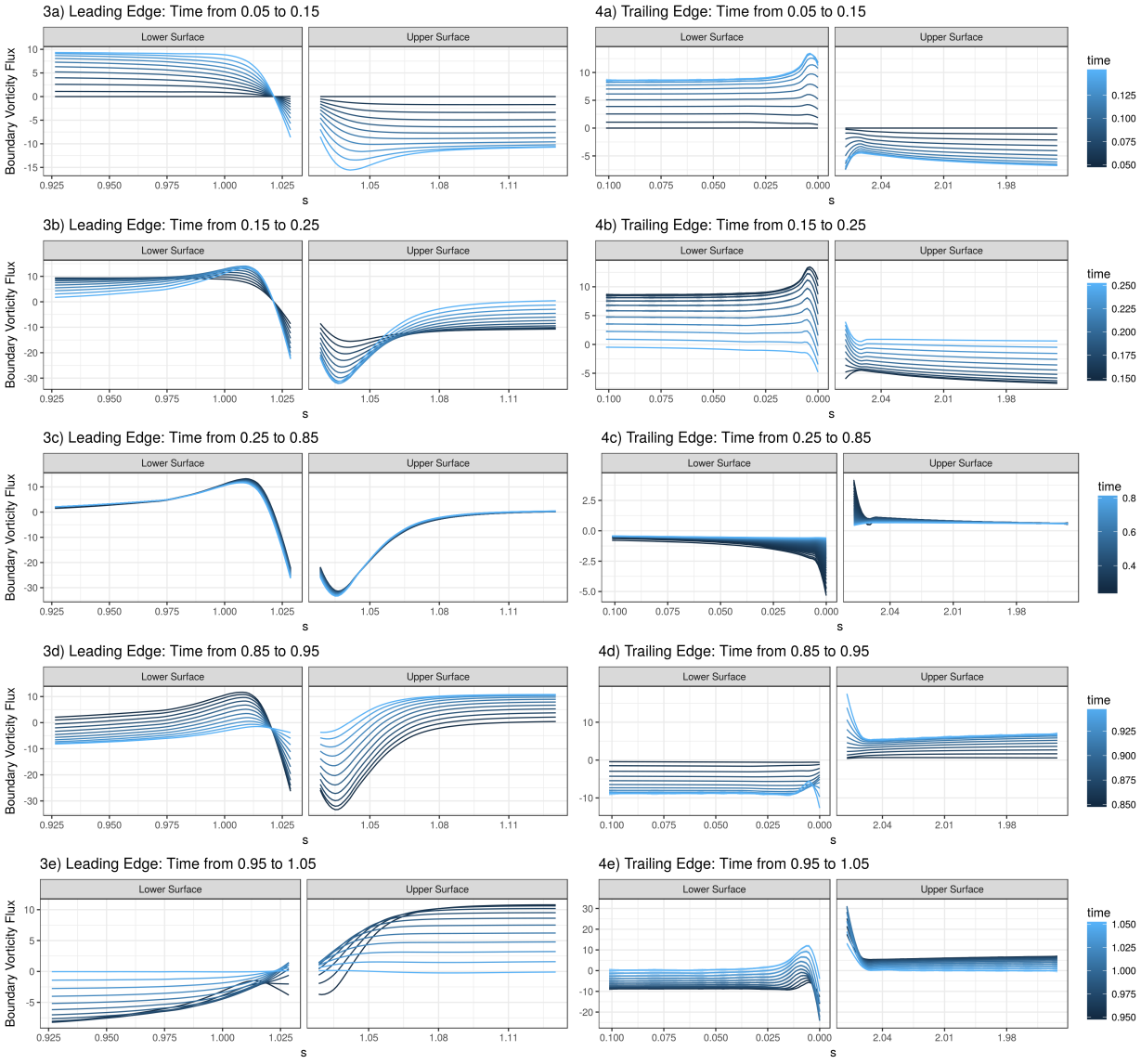

Figure 8: Vorticity production on the airfoil surface for the first and last 10% of the chord